Proceedings of 20th International Congress on Acoustics, ICA 2010

23–27 August 2010, Sydney, Australia

Improving the resolution of beamforming measurements on wind turbines

Angeliki Xenaki, Finn Jacobsen, Elisabet Tiana-Roig and Efrén Fernández Grande

Acoustic Technology, Department of Electrical Engineering, Technical University of Denmark, Lyngby, Denmark

PACS: 43.60.Fg, 43.28.We, 43.50.Yw

ABSTRACT

The spatial resolution of a beamformer based on a planar microphone array in a measurement plane parallel to the array can be approximated by a two-dimensional convolution of the actual distribution of incoherent sources and the beamformer's response to a point source. Several methods are available for deconvolving the resulting blurred picture and thus improving the resulting resolution. This investigation is concerned with a similar deconvolution for the three-dimensional case.

INTRODUCTION

Near field beamforming with a planar phased array of microphones is an attractive technique for locating sound sources at intermediate distances from the array [1]. However, the method has some inherent limitations, including spatial resolution constraints and effects of sidelobes. On certain conditions it is possible to 'clean' the beamformer map and thus improve the spatial resolution and suppress sidelobe effects. For example, when some requirements are met it is possible to improve the beamformer response ('clean the dirty map') using deconvolution algorithms. Moreover, this deconvolution can be carried out using spectral methods, which is computationally advantageous. However, the use of deconvolution for improving the beamformer response implies that its response to a point source depends only on the distance between the focus point of the beamformer and the position of the point source. This property is called 'shift invariance'. This is usually only approximately the case. However, there are reasons to believe that improved shift invariance can be obtained using a transformed set of coordinates. The purpose of this paper is to examine the matter.

BEAMFORMING AND NEAR FIELD SOURCE IMAGING

Beamforming involves sampling the sound pressure with spatially distributed transducers, and post-processing the data by a digital procedure that scans the scene of interest for sound sources. In conventional delay-and-sum beamforming this steering is achieved by applying appropriate delays to the pressure signals from the transducers followed by a summation of all the delayed signals. This procedure results in the coherent addition of signals coming from the direction of focus, maximising the energy in the beamformer output, whereas signals from other directions will be attenuated, leading to a specific beamformer directivity pattern [2].

If the sound source is sufficiently far from the array the resulting sound field sampled by the array may be regarded as a plane wave. In this case the purpose of the beamforming is to detect the direction of the propagating wave; see Figure 1, which illustrates a planar microphone array exposed to an incident plane wave.

The individual delay τ_m applied to the signal recorded by the

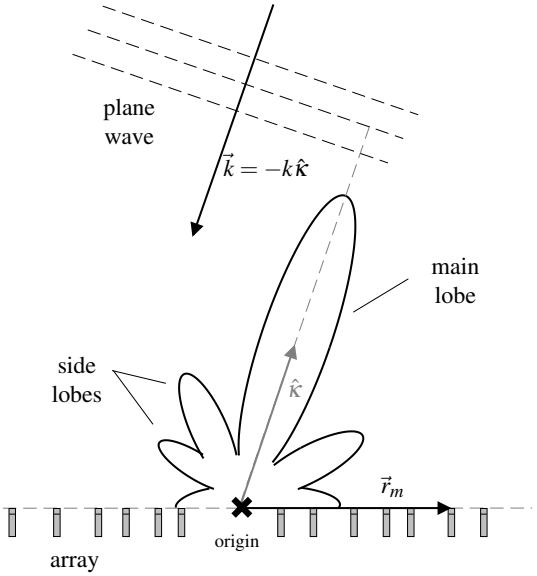

Figure 1: Far field beamforming for detecting the direction of a distant sound source.

m'th transducer for focusing the beam towards the direction defined by the unit vector $\hat{\kappa}$ is related to the position of the transducer $\vec{r}_m$ and the speed of sound c (here assumed to be constant) [3],

$$\tau_m = \frac{\hat{\kappa} \cdot \vec{r}_m}{c}. \tag{1}$$

Expressed in the frequency domain the beamformer output becomes

$$\begin{aligned} B(\hat{\kappa}, \omega) &= \frac{1}{M} \sum_{m=1}^{M} w_m P_m(\omega) e^{-j\omega\tau_m} \\ &= \frac{1}{M} \sum_{m=1}^{M} w_m P_m(\omega) e^{j\vec{k}\cdot\vec{r}_m}, \end{aligned} \tag{2}$$

where w_m is a weighting factor applied to each individual microphone signal $P_m(\omega)$, and $\vec{k}$ is the wavenumber vector that

corresponds to the direction of propagation of the expected plane wave (see Figure 1). With an incident plane wave propagating in a direction given by the wavenumber vector $\vec{k}_0$ the pressure signals are

$$P_m(\omega) = P_0 \cdot e^{-j\vec{k}_0 \cdot \vec{r}_m}, \tag{3}$$

and it can now be seen that the phases cancel out and the beamformer output assumes a maximum value if it is steered in the right direction. By steering the beam successively in all possible directions, the directions of possible point sources are revealed.

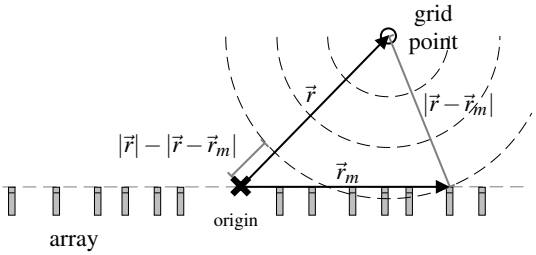

Figure 2: Near field beamforming for mapping sound source locations.

If a sound source is expected at an intermediate distance from the array the beamformer should be focused at exact positions in space rather than in directions, and the curvature of the propagating spherical waves has to be taken into account; see Figure 2, which illustrates how the wavefronts arrive at the various microphone positions. In this case the individual time delays required for aligning the signals are given by

$$\tau_m = \frac{|\vec{r}| - |\vec{r}-\vec{r}_m|}{c}. \tag{4}$$

Expressed in the frequency domain the array response becomes

$$B(\vec{r},\omega) = \frac{1}{M}\sum_{m=1}^{M} w_m P_m(\vec{r},\omega) e^{-jk(|\vec{r}|-|\vec{r}-\vec{r}_m|)}, \tag{5}$$

where $P_m(\vec{r},\omega)$ is the sound pressure at the position of the m'th microphone,

$$P_m(\vec{r},\omega) = P_0 \cdot \frac{e^{-jk|\vec{r}-\vec{r}_m|}}{|\vec{r}-\vec{r}_m|}. \tag{6}$$

In a stationary sound field the mean square output of the beamformer can be expressed in terms of a sum of cross-spectra [3],

$$\begin{aligned}\overline{|B(\vec{r},\omega)|^2} = &\frac{1}{M^2}\sum_{m=1}^{M} w_m^2 C_{mm} \\ &+ \frac{1}{M^2}\sum_{m\neq n}^{M} w_m w_n C_{mn} e^{-jk(|\vec{r}-\vec{r}_m|-|\vec{r}-\vec{r}_n|)},\end{aligned} \tag{7}$$

where C_{mn} is the cross-spectral matrix given by

$$C_{mn} = \overline{P_m^*(\omega)\cdot P_n(\omega)}. \tag{8}$$

The beamformer response can be improved if an amplitude correction that takes account of the attenuation of the spherical wave sound field at the various transducers is incorporated. This problem has been addressed by Christensen and Hald [4]; their solution is based on minimising an error function between the measured and the modelled cross-spectra C_{mn} with respect to amplitudes. The resulting optimal imaging function is

$$I^2(\vec{r},\omega) = \frac{1}{M}\frac{\left|\sum_{m,n=1}^{M} C_{mn}(\omega) v(\vec{r}-\vec{r}_m) v^*(\vec{r}-\vec{r}_n)\right|}{\sqrt{\sum_{m,n=1}^{M} |v(\vec{r}-\vec{r}_m)|^2 |v(\vec{r}-\vec{r}_n)|^2}}, \tag{9}$$

where v is the steering vector, defined by

$$v(\vec{r}) = \frac{e^{-jk(|\vec{r}|)}}{|\vec{r}|}. \tag{10}$$

Excluding the autospectra in the diagonal of the matrix in cross-spectral beamforming tends to reduce the sidelobe level [4]. In this case the imaging function takes the form

$$J^2(\vec{r},\omega) = \frac{1}{\sqrt{M(M-1)}}\frac{\left|\sum_{m\neq n}^{M} C_{mn}(\omega) v(\vec{r}-\vec{r}_m) v^*(\vec{r}-\vec{r}_n)\right|}{\sqrt{\sum_{m\neq n}^{M} |v(\vec{r}-\vec{r}_m)|^2 |v(\vec{r}-\vec{r}_n)|^2}}. \tag{11}$$

The results presented in what follows are based on this expression. Finally it should be mentioned that random non-redundant array geometries tend to reduce aliasing effects due to periodicities in the array pattern [5].

CONVOLUTIONAL FORMULATION OF THE PHASED ARRAY RESPONSE

In order to obtain an image of the sound source distribution within the scene of interest, a beamforming procedure is implemented that involves scanning the observation space by steering successively at a grid of equidistant points. In principle this maps the relative contributions of the sound sources that are present in the scanned region. The mean square response of the beamformer to a point source with unit strength placed at an arbitrary position in the observation grid is called the 'point spread function', p. This is the squared spatial impulse response of the beamformer and reveals its directivity characteristics and resolution capabilities.

The presence of uncorrelated sources at arbitrary positions in the observation grid, $\vec{r}'$, gives rise to a mean square beamformer response that can be written as

$$\overline{|b(\vec{r})|^2} = \sum_{\vec{r}'} q(\vec{r}') \cdot p(\vec{r}|\vec{r}'), \tag{12}$$

where q is the strength of the sources and $\vec{r}$ and $\vec{r}'$ are vectors that denote the current focus point and the position of the point source in the grid, respectively.

The point spread function is shift invariant if it depends only on the distance between the current observation point and the source position and not on the individual positions *per se*. This is generally the case only when the source region is small compared with the distance between the array and the source, and this is the case only if the beamformer map is limited to a relatively small 3D region. In this case the point spread function takes the form:

$$p(\vec{r}|\vec{r}') = p(\vec{r}-\vec{r}'), \tag{13}$$

and eq. (12) can now be expressed as a convolution,

$$\overline{|b(\vec{r})|^2} = \sum_{\vec{r}'} q(\vec{r}') \cdot p(\vec{r}-\vec{r}') = q * p, \tag{14}$$

which in turn makes it possible to calculate the beamformer output in the wavenumber domain making use of the computational advantage of a discrete spatial Fourier transform,

$$\overline{|b(\vec{r})|^2} = F^{-1}\left[F[q]\cdot F[p]\right], \tag{15}$$

where F denotes a three-dimensional Fourier transform and F^{-1} denotes the corresponding inverse transform. However, it should be emphasised that the validity of eq. (15) is restricted to the case where the sources are incoherent and the point spread function is shift invariant.

DECONVOLUTION ALGORITHMS AND SPECTRAL METHODS

In the ideal case the point spread function would be a delta function, and the beamformer output would reveal the location of sources within the region of observation directly. Unfortunately this is never the case since the array geometry imposes certain resolution limitations and gives rise to sidelobes. Hence, there is a need of improving the map by post-processing.

Deconvolution techniques are widely used in many fields of imaging for 'cleaning' the obtained maps. An investigation on the application of various iterative deconvolution algorithms in aeroacoustic beamforming measurements has been carried out by Ehrenfried and Koop [6]. Several algorithms were compared in terms of computational load, robustness and limitations, using synthesised data. The tested algorithms were non-negative least-squares solvers aiming to converge towards the actual source distribution (in two dimensions) through an iterative procedure. The investigation included the classical deconvolution algorithms that involve matrix operations to solve eq. (12) under the constraint of non-negative source strengths. The same algorithms were also modified to incorporate spectral procedures providing the possibility of using a discrete spatial Fourier transform to perform the operations in the wavenumber domain. This tends to reduce the computational effort dramatically compared with the classical methods resulting in a significantly increased calculation speed. However, the Fourier based methods require by definition a shift invariant point spread function, and it is difficult to meet such requirements in typical setups in aeroacoustic measurements. One possibility is simply to ignore the variations of the point spread function across the observation grid, which in this case must be restricted to a very limited region. Another solution, proposed by Ehrenfried and Koop [6], involves nesting the Fourier based algorithm into another iterative procedure that accounts for the variations of the point spread function as the point source is shifted across the observation grid. This method is expected to converge to an accurate solution of the source distribution. However, the nesting of iterative procedures tends to slow down the process significantly, and the computational effort becomes comparable to the one of the classical methods.

The so-called DAMAS2 algorithm suggested by Dougherty [7] (which is an extension of the original DAMAS deconvolution algorithm introduced by Brooks and Humpreys [8]) seems to be a promising compromise between accuracy and computational efficiency considering the fact that the task involves scanning a three-dimensional region. The DAMAS2 algorithm gives good results if the assumption of a shift invariant point spread function is met, and it provides the possibility of regularising the process by incorporating a Gaussian spatial low-pass filter to suppress high wavenumber noise, such as noise leaking into the reconstructed map due to transducer phase mismatch or the presence of strong point sources outside the region of interest.

The DAMAS2 algorithm comprises the following steps:

- The point spread function is computed under the assumption of shift invariance based on eq. (13).
- The sum of the point spread function at positions across the observation grid is stored in a constant,

$$\alpha = \sum_{\vec{r}} p(\vec{r} - \vec{r}'). \tag{16}$$

- A Gaussian regularisation filter is computed,

$$\psi(\vec{k}) = \exp\left(-\ln(2)\frac{\left|\vec{k}\right|^2}{k_c^2}\right), \tag{17}$$

  where k_c is the spatial cutoff frequency.

- The iterative procedure starts. Initialisation of the source strengths with zeros is assumed. In each iteration cycle (i) the beamformer output is estimated through a spectral procedure in the wavenumber domain based on the point spread function and the assumed source distribution at the same cycle,

$$\bar{b}(\vec{r})^{(i)} = F^{-1}\left[F\left[q(\vec{r})^{(i)}\right] \cdot F\left[p(\vec{r})\right] \cdot \psi(\vec{k})\right]. \tag{18}$$

- An update of the estimated source distribution is constructed subject to the constraint of non-negative strength values,

$$q(\vec{r})^{(i+1)} = \max\left(q(\vec{r})^{(i)} + \frac{b(\vec{r}) - \bar{b}(\vec{r})^{(i)}}{\alpha}, 0\right). \tag{19}$$

- The last two steps are repeated until the process converges by minimisation of the residuals of the actual and estimated beamformer response in eq. (19). It is apparent that each iteration cycle necessitates the calculation of only one Fourier transform and one inverse transform since the point spread function is regarded as shift invariant and can be transformed one single time.

The sidelobe levels are gradually minimised by the iterative procedure described above, eventually resulting in a 'clean' beamforming map where the effects of ghost sources are reduced and the real source distribution is reconstructed more accurately.

COORDINATE TRANSFORMATION

The potentially improved beamforming maps obtained after application of iterative deconvolution algorithms combined with the computational advantages of the fast spectral procedures constitute obvious solutions for accurate source location in three-dimensional acoustic sound source imaging. However, by definition such procedures require the point spread function to be shift invariant. Aeroacoustic measurements for locating sound sources within a predefined observation region often involve configurations where spatially extended sources are in the near field region of the microphone array. In such cases the point spread function depends on the actual position of the source in the observation grid, and the prerequisite for the convolutional formulation of the beamformer output is only approximately fulfilled.

In order to obtain a more convolutional form of the beamformer response, an unconventional set of coordinates for defining the focal points on the observation grid is introduced. The new grid is determined by equidistant points in the new coordinate system instead of in the Cartesian one and is defined so as to circumscribe the area of interest. This transformation of coordinates aims at making the point spread function retain its characteristics irrespectively of the location of the corresponding point source in the observation grid. Such techniques are a common practice in underwater acoustic vision performed with digital beamforming [9], [10], and a similar transformation for near field aeroacoustic measurements has been suggested by Dougherty [7].

To perform three-dimensional beamforming two angles, ϕ and θ, are required to define the steering directions as shown in Figure 3. Note that these angles differ from the conventional azimuth and polar (or elevation) angle.

The steering directions are equally spaced in the sines of the two angles, and the vector that determines the position of the

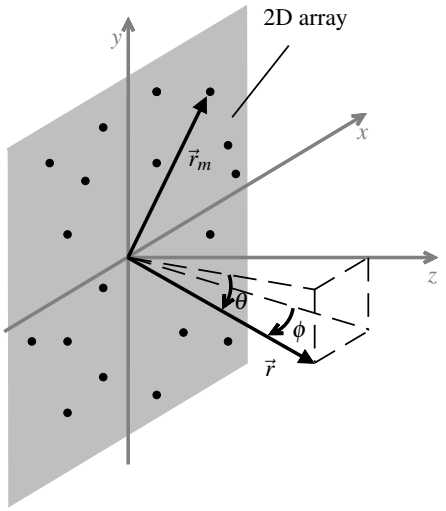

Figure 3: Steering a beamformer in 3D space.

current focal point in the observation grid is defined through the set of coordinates

$$\begin{aligned}(x,y,z) &= r\cdot\left(\sin\phi,\sin\theta,\sqrt{\cos^2\phi-\sin^2\theta}\right)\\ &= r\cdot\left(u,v,\sqrt{1-u^2-v^2}\right),\end{aligned} \tag{20}$$

where the last substitution is based on the transformation

$$u=\sin\phi=\frac{x}{r},\ v=\sin\theta=\frac{y}{r},\ w=\frac{z_{min}}{r},\ r=|\vec{r}|\,, \tag{21}$$

in which z_{min} is the minimum axial distance within the region of validity, defined in ref. [11]. Obviously the variables u and v range between -1 and 1, whereas the variable w takes non-negative values up to unity. The reason for introducing the variable w will become apparent in the following.

The transition of the point spread function to a convolutional formulation when it is calculated through the new set of coordinates becomes more intuitively clear if one inspects the delays applied to the individual transducers of the array in order to steer the beam to a specific direction.

Assuming that the microphone array is lying on the ground and the origin of the coordinate system coincides with the centre of the array, the position of the m'th transducer is defined by the vector $\vec{r_m}=(x_m,y_m,0)$. The difference in travel time between a transducer placed at $\vec{r_m}$ and another placed at the centre of the array at the position $\vec{r_0}=(0,0,0)$ is $(|\vec{r'}-\vec{r_m}|-|\vec{r'}|)/c$ when the beam is focused at a point in the grid at $\vec{r'}=(x',y',z')$ that coincides with the correct point source location, and $(|\vec{r}-\vec{r_m}|-|\vec{r}|)/c$ when the beam is focused towards a mismatched grid point (with no source) at $\vec{r}=(x,y,z)$. It follows that the point spread function depends on the quantity

$$c\cdot\tau=\left(|\vec{r}-\vec{r_m}|-|\vec{r}|\right)-\left(\left|\vec{r'}-\vec{r_m}\right|-\left|\vec{r'}\right|\right). \tag{22}$$

By replacing the Cartesian coordinates that define the position vectors according to the transformation described by eq. (20), eq. (22) can be written as

$$\begin{aligned}c\cdot\tau=&-x_m(u-u')-y_m(v-v')\\ &+\frac{1}{2}(x_m^2+y_m^2)\left(\frac{1}{r}-\frac{1}{r'}\right).\end{aligned} \tag{23}$$

Equation (23) is based on a second order binomial expansion of the square root. However, this approximation holds only under certain assumptions that define the region of validity [11]. The near field beam pattern is limited within an angular region of no more than 18° off the z-axis and in a maximum range defined by the frequency and the array dimensions. These limitations reduce the flexibility of the method. The last term in eq. (23) accounts for effects of the curvature of the spherical waves and defines the range resolution. This is generally improved with larger array apertures, and the maximum and minimum value of the range vary with the aperture [2]. By introducing the variable w instead of the range term in eq. (23) the resulting expression attains the shift invariant form,

$$c\cdot\tau=-x_m(u-u')-y_m(v-v')+\frac{1}{2}\frac{x_m^2+y_m^2}{z_{min}}(w-w'). \tag{24}$$

The last expression has the convolutional form of the point spread function as defined in eq. (13) within an appropriate region of validity.

SIMULATION RESULTS

In order to examine the possibility of applying deconvolution methods to improve the resolution in delay-and-sum beamforming measurements on wind turbines a simulation model has been implemented based on the theory presented in the foregoing. The configuration is a scaled version of the actual one used for wind turbine measurements and is also examined experimentally in the controlled environment of an anechoic chamber.

The configuration, shown in Figure 4, consists of a planar aperture with a diameter of 1 m with sparsely distributed microphones in a pseudorandom pattern and two pairs of uncorrelated point sources.

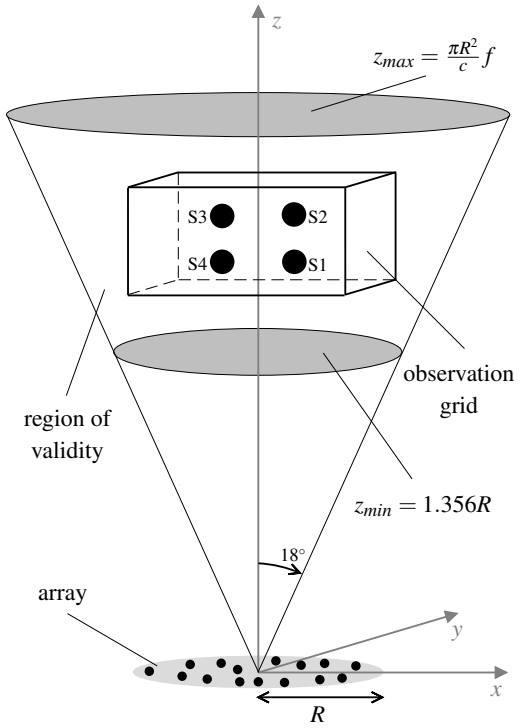

Figure 4: Test configuration with a planar sparse array. Four omnidirectional sources of equal strength are placed within the observation grid in 3D space. The region of validity is the space where near field beamforming can be performed using the transformed set of variables.

The relative microphone array position and extent combined with the frequency range of concern set the limits for near field beamforming in the transformed set of coordinates [11]. In what follows a frequency of 6000 Hz is considered, corresponding to a fairly large near field region with the given array aperture. The idea of the two pairs of point sources is to examine both the lateral and the range resolution of the array. The origin of the coordinate system is identified at the geometrical centre of the array. The two pairs of sources are positioned at two different range distances, and the sources of each pair are symmetrically spaced from the origin of the coordinate system in the *x*-axis and shifted towards one side of the *y*-axis. This configuration has been chosen in order to comply with an actual wind turbine measurement setup. In the real measurements the microphone array will be placed on the ground at a small distance from the base of the installation, and the sound sources are expected to appear as uncorrelated aeroacoustic noise along the leading and trailing edge of the wing.

All sources have the same strength. Figure 5 shows the distribution of the four sources in the conventional Cartesian coordinate system (Figure 5a) and in the transformed one (Figure 5b). As the coordinate transformation described by eq. (21) implies, the more distant the location of the sources is in the Cartesian coordinate system, the closer to the origin of the *uvw*-coordinate system they will appear. Thus even though all sources lie in the same *xz*-plane they will appear in different *uw*-planes. Similarly, the source pairs S1, S2 and S3, S4 that are set to the same *yz*-planes will appear in different *vw*-planes in the transformed coordinate system.

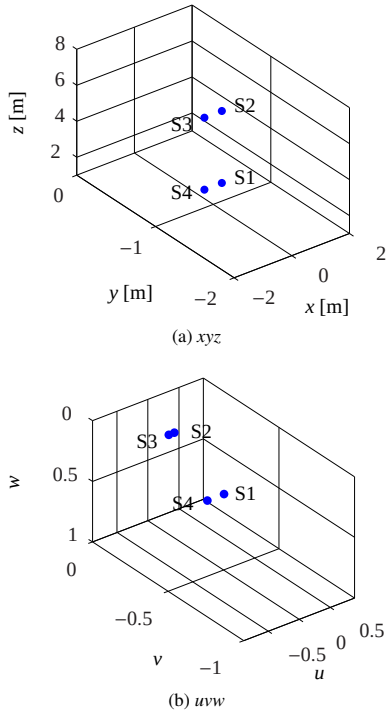

(a) *xyz*

(b) *uvw*

Figure 5: Source distribution in Cartesian coordinates (top) and in the *uvw*-coordinates.

The translational characteristics of the point spread function both in the conventional and the transformed set of coordinates are presented in Figures 6 and 7. Figure 6 refers to a plane parallel to the microphone array while Figure 7 refers to a plane perpendicular to the microphone array.

Comparison of the beamformer's response to different point source locations in the transformed coordinates reveals that

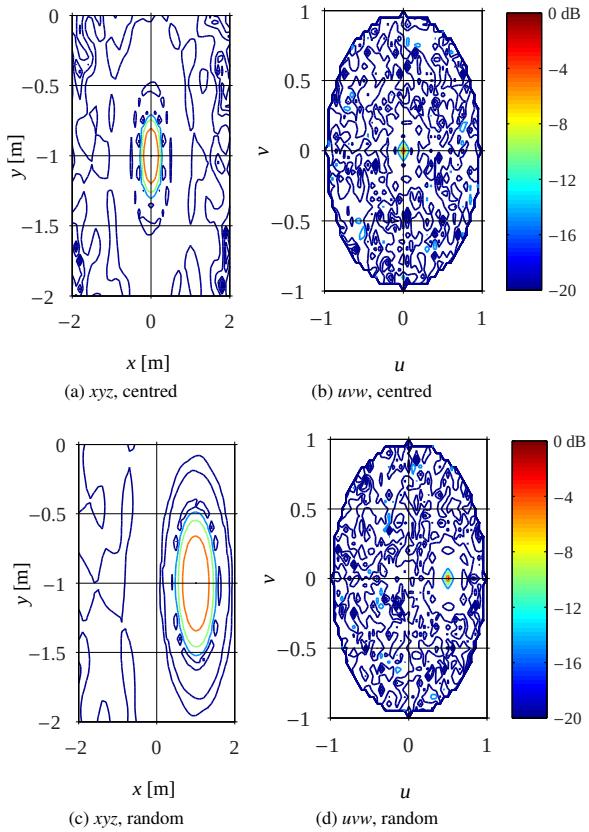

(a) *xyz*, centred

(b) *uvw*, centred

(c) *xyz*, random

(d) *uvw*, random

Figure 6: Comparison of the point spread function in the two different coordinate systems in a plane parallel to the array for a centred point source position (top) and for a random point source position (bottom).

the point spread function retains its form irrespectively of the position of the point source in the observation grid (Figures 6b, 6d, 7b, 7d). Conversely, when beamforming is performed according to a grid defined in Cartesian coordinates the point spread function alters its characteristics: the main lobe becomes wider due to the transition of the source to more distant positions and tilted in the perpendicular plane due to transition of the source to off-axis positions (Figures 6a, 6c, 7a, 7c). Consequently, the point spread function has a more shift invariant form in the new set of coordinates.

The 3 dB width of the main lobe of the point spread function dictates the limitation in the minimum spatial separation of sources that can be resolved through the beamforming procedure according to the Rayleigh criterion [3]; see Figure 8. The shift invariance of the point spread function implies that the resolution is constant in the *uvw*-domain irrespectively of the source position. However, the inverse transform to the Cartesian system of the processed data will result in poorer resolution as the range of the source increases.

First, the beamformer output is calculated by applying the classical delay-and-sum procedure in an equidistantly spaced observation grid in the Cartesian coordinate system. Figure 9 shows the results in three planes, one perpendicular to the array and two parallel to the array, where the sources are expected. It is apparent that the further from the array the source location, the poorer the resolution. In addition, the resulting map is contaminated with sidelobe effects that appear as weaker 'ghost' sources.

The corresponding beamformer output resulting from scanning

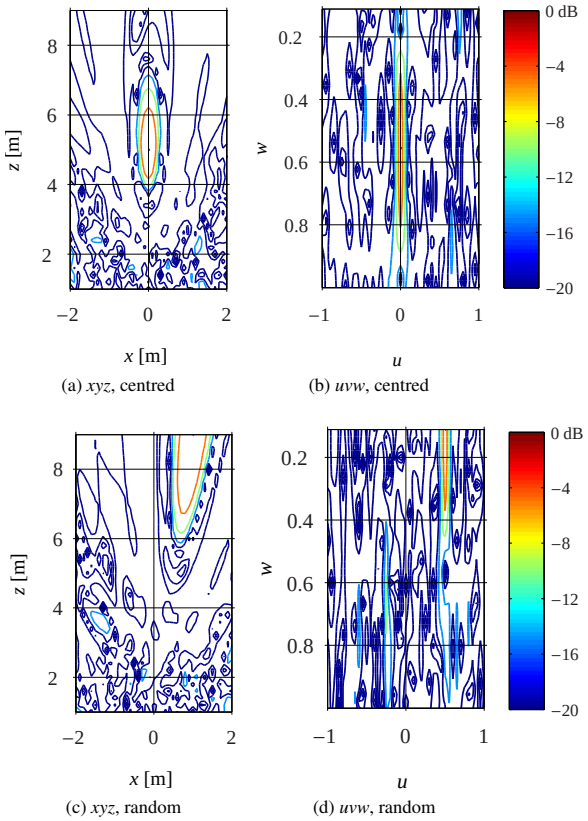

(a) *xyz*, centred (b) *uvw*, centred

(c) *xyz*, random (d) *uvw*, random

Figure 7: Comparison of the point spread function in the two different coordinate systems in a plane perpendicular to the array for a centred point source position (top) and for a random point source position (bottom).

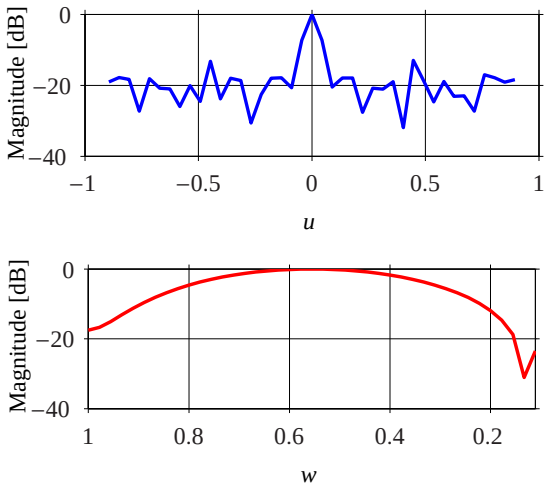

Figure 8: Point spread function in the *uvw*-coordinate system in a plane perpendicular to the array for a centred point source position as a function of *u* and *w*.

the observation grid through the transformed coordinates by a delay-and-sum procedure and then inversely transforming the results to the Cartesian system is presented in Figure 10. The inverse transform is necessary in order to 'translate' the obtained data from an equidistantly spaced grid in the *uvw*-domain to an equidistantly spaced grid in the *xyz*-domain and is based on a linear interpolation. Comparison of the results demonstrates significantly improved resolution when the beamforming procedure is implemented in the *uvw*-coordinate system.

Post-processing the beamforming data by application of the

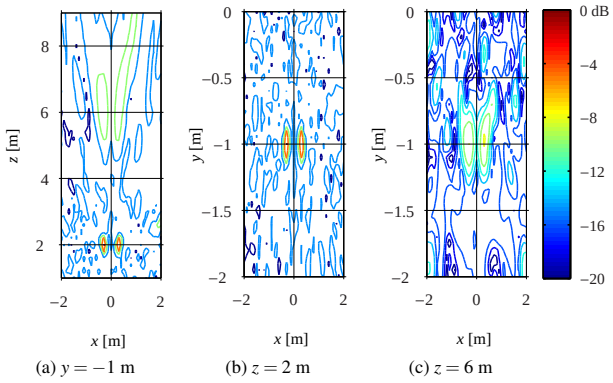

(a) $y = -1$ m (b) $z = 2$ m (c) $z = 6$ m

Figure 9: Beamformer output using the delay-and-sum procedure in the Cartesian coordinate system.

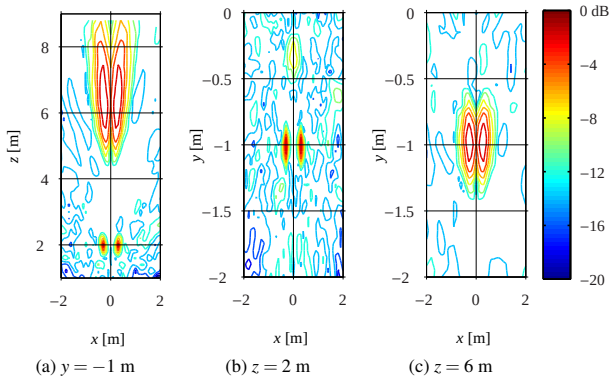

(a) $y = -1$ m (b) $z = 2$ m (c) $z = 6$ m

Figure 10: Beamformer output by applying the delay-and-sum procedure in the transformed *uvw*-coordinate system.

DAMAS2 deconvolution algorithm results into the reconstructed source distribution depicted in Figure 11. It can be seen that the sidelobes have vanished completely from the reconstructed source map. In addition the resolution has been improved, resulting in a more accurate identification of the source positions and their relative strength.

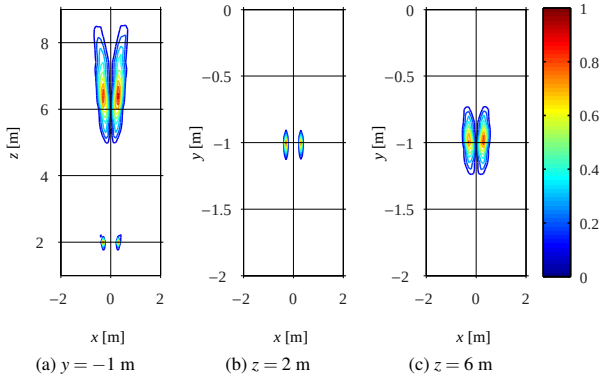

(a) $y = -1$ m (b) $z = 2$ m (c) $z = 6$ m

Figure 11: Reconstructed source distribution and relative strengths after applying the spatial deconvolution algorithm.

EXPERIMENTAL RESULTS

In order to validate the simulation results presented in the foregoing, some experiments have been carried out in an anechoic room with a volume of around 1000 m^3. The configuration depicted in Figure 4 was established, and the sound pressure was recorded from 60 microphones sparsely distributed on an array with a diameter of 1 m. The cross-spectral matrix was estimated

from records of 10 seconds' duration. Next, the delay-and-sum beamforming procedure was applied to scan electronically the scene of interest. In the same way as in the simulation study, the beamformer output was determined by scanning across an equidistantly spaced grid in Cartesian coordinates as well as across an equidistantly spaced grid in the transformed coordinate system. Finally, the reconstructed source distribution resulting from 'cleaning' the beamforming map with a deconvolution procedure was calculated. The results are depicted in Figures 12, 13 and 14.

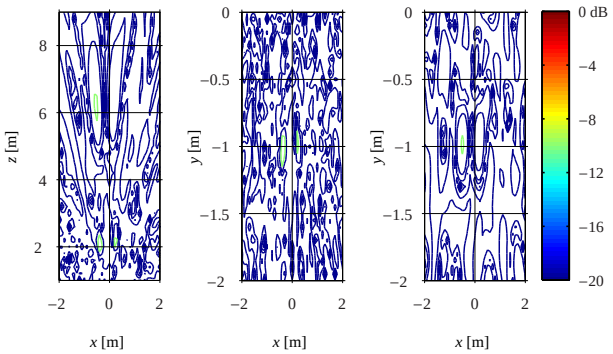

(a) $y = -1$ m (b) $z = 2$ m (c) $z = 6$ m

Figure 12: Beamformer output based on experimental data determined using the delay-and-sum procedure in the Cartesian coordinate system.

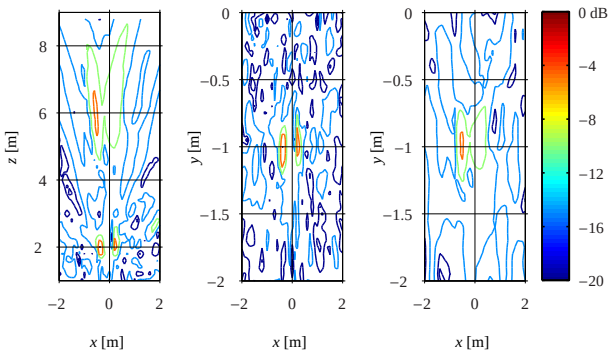

(a) $y = -1$ m (b) $z = 2$ m (c) $z = 6$ m

Figure 13: Beamformer output based on experimental data determined using the delay-and-sum procedure in the transformed *uvw*-coordinate system.

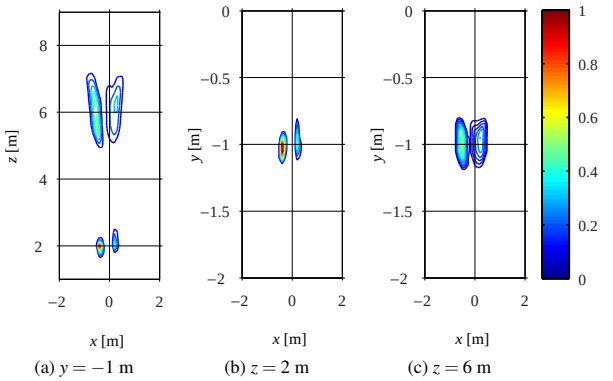

(a) $y = -1$ m (b) $z = 2$ m (c) $z = 6$ m

Figure 14: Reconstructed source distribution and relative strengths after applying the spatial deconvolution algorithm to the experimental data.

In agreement with the results of the simulation study, the beamformer map is already improved in terms of resolution when the steering points are defined in the transformed *uvw*-coordinate system. Moreover, the deconvolution procedure results in a 'clean' imaging map, free of sidelobe effects. A slight mismatch of the source locations between the simulated and the experimental case is probably due to the difficulties in fine tuning the source positions in the experimental setup with the provided equipment. Furthermore, the fact that the source strengths are not fully reconstructed is attributed to the rather short time records used in the measurements. Nevertheless, the agreement between the simulation study and the experimental results validate the applicability of the method.

CONCLUSIONS

An investigation of the possibility of improving the resolution of 3D beamforming based on a planar microphone array by deconvolution methods has been carried out. The computational advantage of incorporating spectral procedures to the deconvolution requires a shift invariant point spread function. However, in near field beamforming, the beamformer's response to a point source depends on the individual position of the source within the observation grid. A more shift invariant form of the point spread function is achieved by introducing an unconventional set of coordinates for defining the focal points in the observation grid. The validity of this approach has been examined by a simulation study as well as by experimental results. Both simulations and experimental results demonstrate a significant improvement of the beamformer output in terms of enhanced resolution and reduced sidelobe contamination.

ACKNOWLEDGEMENTS

The authors would like to thank Brüel & Kjær for lending us a microphone array with 60 microphones and other equipment for the experimental part of this investigation.

REFERENCES

[1] Yong Thung Cho, M.J. Roan, and J.S. Bolton. "Comparison of near-field beamforming and acoustical holography for sound source visualization". *Journal of Mechanical Engineering Science* **223** (2009), pp. 819–834.

[2] D.H. Johnson and D.E. Dudgeon. *Array Signal Processing*. Prentice Hall, 1993.

[3] J.J. Christensen and J. Hald. "Beamforming". *Brüel & Kjær Technical Review* **1** (2004).

[4] J.J. Christensen and J. Hald. "Improvements of cross spectral beamforming". *32nd International Congress and Exposition on Noise Control Engineering (InterNoise 2003)*. 2003.

[5] J. Hald and J.J. Christensen. "A novel beamformer array design for noise source location from intermediate measurement distances". *Journal of the Acoustical Society of America* **112** (2002), pp. 2448–2448.

[6] K. Ehrenfried and L. Koop. "A comparison of iterative deconvolution algorithms for the mapping of acoustic sources". *AIAA Journal* **45** (2007), pp. 1584–1595.

[7] R.P. Dougherty. "Extensions of DAMAS and benefits and limitations of deconvolution in beamforming". *11th AIAA/CEAS Aeroacoustics Conference*. Vol. 3. AIAA. 2005, pp. 2036–2048.

[8] T.F. Brooks and W.M. Humphreys. "A deconvolution approach for the mapping of acoustic sources (DAMAS) determined from phased microphone arrays". *Journal of Sound and Vibration* **294** (2006), pp. 856–879.

[9] M. Palmese and A. Trucco. “Three-dimensional acoustic imaging by chirp zeta transform digital beamforming”. *IEEE Transactions on Instrumentation and Measurement* **58** (2009), pp. 2080–2086.

[10] M. Palmese and A. Trucco. “Digital near field beamforming for efficient 3-D underwater acoustic image generation”. *IEEE International Workshop on Imaging Systems and Techniques - IST 2007*. 2007, pp. 33–37.

[11] L.J. Ziomec. “Three necessary conditions for the validity of the Fresnel phase approximation for the near-field beam pattern of an aperture”. *IEEE Journal of Oceanic Engineering* **18** (1993), pp. 73–76.